J. Phys. D: Appl. Phys. **33** (2000) 3033–3040. Printed in the UK PII: S0022-3727(00)15773-0

Geometrical optical model of the image formation in Makyoh (magic-mirror) topography

Ferenc Riesz

Hungarian Academy of Sciences, Research Institute for Technical Physics and Materials Science, PO Box 49, H-1525 Budapest, Hungary

E-mail: riesz@mfa.kfki.hu

Received 25 July 2000

Abstract. A geometrical optical model for the image formation of Makyoh (or magic-mirror) topography is presented. General relations are given on the optical settings. The basic equations of the imaging are derived. Fundamental features of the imaging are pointed out, and optimum working conditions are established. Simulations of the image of an isolated defect (hillock or depression) and a periodic (sinusoidal) surface are presented for different optical settings. Supporting experimental images are presented.

1. Introduction

The word Ma-kyoh (meaning 'magic mirror' in Japanese) refers to a bronze mirror originating from ancient China that reflects an image to a distant wall when the Sun shines on the mirror. A relief pattern, resembling the projected image, is engraved on the back side of the mirror; no pattern can be seen on the front side by the naked eye [1]. The 'magic' of the mirror can be understood using simple geometrical principles: the local irregularities of the reflecting surface act as concave or convex mirrors therefore a collimated light beam impinging on the surface produces an image on a screen that, to a certain extent, reflects the mirror's morphology. The front-face microdeformations (invisible to the naked eye) are caused by the stresses due to the engraved back image.

The Makyoh concept proved to be a powerful topographic tool for the characterization of the morphology of mirror-like surfaces, such as semiconductor wafers [2]. The reported sensitivity of the method is a 0.4 μm height difference over a 10 mm distance and 50 nm over a 0.5 mm distance [3]. Makyoh topography has proven its power, for example in detecting flaws induced by wafer slicing, polishing and lapping [4, 5] and defects in directly bonded Si wafers [6]. Makyoh-topography instruments are also available commercially.

Makyoh gained its success due to its extreme instrumental simplicity, low cost and real-time operation. However, the interpretation of Makyoh images is not straightforward. It is generally accepted and proved by surface-stylus profiling and laser interferometry [6] that the image is related to the surface morphology; however, no comprehensive theory exists for the image formation. Only a Monte Carlo (MC) simulation for some specific cases has allowed us to draw certain general conclusions [7]. This limited knowledge clearly hampers the wider application of the method.

This paper presents a comprehensive geometrical optical model of the Makyoh image formation mechanism, based on the results of Burkhard and Shealy [8, 9], with an aim to provide a solid basis both for the quantitative analysis as well as for the quick, qualitative or semi-quantitative visual interpretation of the images. Preliminary accounts of this work have been published [10]. The paper is organized as follows. In section 2.1, general relations are given on the optical settings; general imaging equations are formulated within the framework of geometrical optics in section 2.2. Fundamental features of the imaging are established in section 2.3. The validity and limits of the geometrical optical approach are discussed in section 2.4, and some secondary effects are treated in section 2.5. Then, one-dimensional simulations of the images of an isolated defect (hillock or depression) and a periodic (sinusoidal) surface are presented in section 3. In section 4, experimental images are shown and compared to surface-stylus measurements; the results are discussed in the light of the model and the simulation results.

2. Description of the model

2.1. Optical scheme of Makyoh instruments

The simplest Makyoh instrument consists only of a point light source and a screen, imitating the original, ancient use of Makyoh ('temple model'). Temple-model systems are characterized by the light source–sample and sample–screen distances (S and L, respectively). More compact instruments utilize additional optical elements to decrease the size of the instrument and to facilitate the use of modern electronic

0022-3727/00/233033+08$30.00

cameras [2]. For any camera-based system, an equivalent temple-model system can be found. The optical elements image the light source and the camera image plane to virtual positions S^* and L^*, respectively, which are parameters that are equal to the S and L parameters of the equivalent temple-model system, respectively. In addition, magnification factors should be introduced to account for the change of light source and image sizes. Standard geometrical optical calculations give S^* and L^* and the corresponding magnifications [11]. It is important to note that L^* is negative for most practical camera-based systems [11], that is, the image plane ('virtual screen') lies behind the sample. In the following, we deal with temple-model systems only.

2.2. Geometrical optical model

From the geometrical optical point of view, Makyoh imaging is a special case of the general problem of calculating the illuminance of an arbitrary receiver surface by the rays emitted by an extended source and deflected by an arbitrary-shaped deflector surface [8, 9]. At this point, we advance the validity of the geometrical optical approach; this will be justified later. The general formulation gives the illuminance in terms of the given arrangement and the geometry of the deflector and receiver surfaces, and is rather complicated [8, 9]. The Makyoh case is special because (1) the source can be regarded as a point source, (2) the deflector is a closely planar surface with height variations much smaller than the ray path lengths (S and L), (3) the receiver surface (the screen) is a plane, usually parallel to the sample (the deflector) and (4) the light incidence and reflection is closely normal to the sample plane. The derivation presented below utilizes the results of [8], but is adopted to our special case and relies heavily on the above approximations.

Consider a temple-model Makyoh system (figure 1). The surface profile is described by $h(\boldsymbol{r})$. The light source is placed at the point (0, 0, S). The screen plane is parallel to the sample plane. Let a ray hit the surface at a point $\boldsymbol{r}$; the reflected ray hits the screen at the point $\boldsymbol{f}(\boldsymbol{r})$. O* denotes the point in the screen plane that lies on the line that interconnects the source and the point $\boldsymbol{r}$ in the sample plane; $\boldsymbol{r}^*$ denotes the vector pointing from O* to the orthogonal projection of the sample point to the screen plane, and $\boldsymbol{f}^*$ is the vector pointing from O* to the screen point hit by the reflected ray. The incident ray, the local surface normal and the reflected ray are coplanar. The local surface normal's orthogonal projection to the screen plane is $-L\,\mathrm{grad}\,h(\boldsymbol{r})$. If S is large enough compared to the sample size, and the surface slopes are small, that is, when the local angle of incidence, φ is small (which holds for most practical cases), the local surface normal halves the vector $\boldsymbol{f}^*$, thus we can write, projecting $\boldsymbol{r}$ to the screen plane (see figure 1),

$$\boldsymbol{f}(\boldsymbol{r}) = 2[\boldsymbol{r}^* - L\,\mathrm{grad}\,h(\boldsymbol{r})] - (\boldsymbol{r}^* - \boldsymbol{r}) \tag{1}$$

The error introduced is smaller than 5% in terms of the length of $\boldsymbol{f}(\boldsymbol{r})$ for $\varphi < 7^\circ$. As $\boldsymbol{r}^* = \boldsymbol{r} \cdot L/S$, after rearranging, we get

$$\boldsymbol{f}(\boldsymbol{r}) = \left(1 + \frac{L}{S}\right)\left(\boldsymbol{r} - \frac{2L}{1 + L/S}\,\mathrm{grad}\,h(\boldsymbol{r})\right). \tag{2}$$

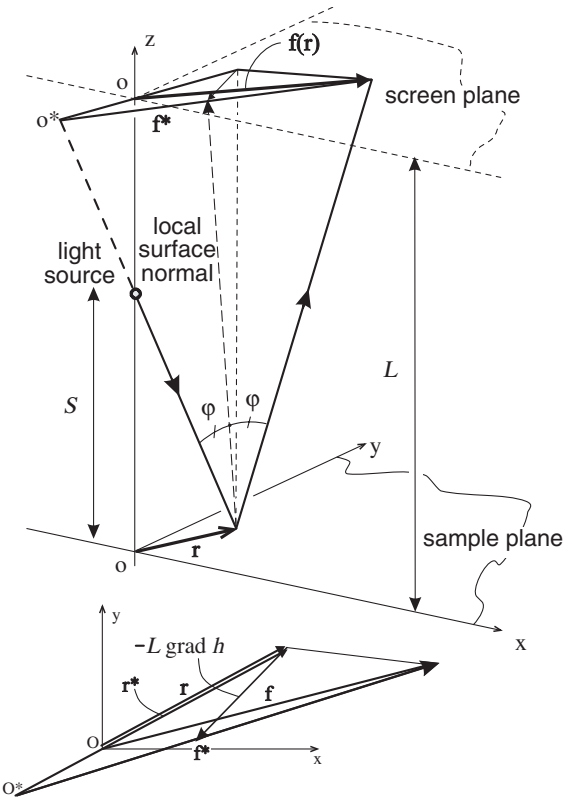

Figure 1. The geometrical optical scheme of Makyoh imaging.

In the special case of $S = \infty$ (parallel beam), equation (2) reduces to:

$$\boldsymbol{f}(\boldsymbol{r})_\infty = \boldsymbol{r} - 2L\,\mathrm{grad}\,h(\boldsymbol{r}). \tag{3}$$

The $I(\boldsymbol{f})$ illuminance of a screen point $\boldsymbol{f}(\boldsymbol{r})$ normalized to that of the corresponding point $\boldsymbol{r}$ of the sample surface is the absolute value of the ratio of the area of the sample surface, $\mathrm{d}A_r$, to that of the screen, $\mathrm{d}A_f$, intersected by an infinitesimal thin reflected light pencil, and multiplied by the sample surface reflectivity $\rho(\boldsymbol{r})$ ($\rho(\boldsymbol{r})$ may incorporate any inhomogeneity of the incident light flux) and the angular factors related to the incidence angles:

$$I(\boldsymbol{f}) = \rho(\boldsymbol{r}) \cos\varphi \cos 2\varphi \left|\frac{\mathrm{d}A_r}{\mathrm{d}A_f}\right|. \tag{4}$$

$\cos\varphi$ and $\cos 2\varphi$ take into account the flux change due to non-normal incidence at the sample and the screen, respectively (as the screen is perpendicular to the z-axis, the angle of incidence at the screen is 2φ). Equation (4) has been evaluated in terms of the intrinsic geometry of the reflecting surface in reference [9]. The result, using our notation, is (see equations (19) and (22) of [9])

$$\begin{aligned} I(\boldsymbol{f}) = \rho(\boldsymbol{r}) \cos 2\varphi \{|1 - 2L(2H\cos\varphi + K_N \tan\varphi \sin\varphi \\ -1/S) + L^2[4K - 2(2H\cos\varphi + K_N \tan\varphi \sin\varphi)/S \\ +1/S^2]|\}^{-1} \end{aligned} \tag{5}$$

where H, K and K_N are the mean, Gaussian and normal curvatures of the surface in the point $\boldsymbol{r}$, respectively [12]. We take the source-to-surface element and surface element-to-screen distances as S and L, however they are slightly larger due to non-normal incidence and reflectance. As φ is small,

the $\tan\varphi \sin\varphi$ terms can be approximated as zero, and $\cos\varphi$ and $\cos 2\varphi$ as unity; thus, after rearrangement, equation (5) reduces to

$$I(\boldsymbol{f}) = \frac{1}{(1+L/S)^2} \frac{\rho(\boldsymbol{r})}{\left|1 - 4H\dfrac{L}{1+L/S} + 4K\left(\dfrac{L}{1+L/S}\right)^2\right|}. \tag{6}$$

The error introduced by the $\varphi = 0$ approximation is second order, since the linear term is zero in the Taylor-series expansion of $I(\boldsymbol{f})$ (equation (5)). The error is the largest when $I(\boldsymbol{f})$ is large; however, this situation, as discussed later, has little practical importance. In the special case of $S = \infty$ (perfectly collimated beam), equation (6) reduces to

$$I(\boldsymbol{f})_\infty = \frac{\rho(\boldsymbol{r})}{|1 - 4HL + 4KL^2|} \tag{7}$$

or in an equivalent form

$$I(\boldsymbol{f})_\infty = \frac{\rho(\boldsymbol{r})}{|(1 - 2LC_{min})(1 - 2LC_{max})|} \tag{8}$$

where C_{min} and C_{max} are the minimum and maximum curvatures of the surface at the point $\boldsymbol{r}$, respectively ($H = (C_{min} + C_{max})/2$ and $K = C_{min}C_{max}$; see [12]).

An important scaling law follows from the comparison of equations (2) and (3), and (6) and (7): in the general case, the linear size of the image as well as L are scaled by the factor $1 + L/S$ as compared to the $S = \infty$ case. Furthermore, the illuminance of a given screen point is scaled down by $(1+L/S)^2$ (see equation (6)). This means that from the point of view of the image formation, one parameter, $L_r = L/(1 + L/S)$, is sufficient to describe all Makyoh systems. This property has not been recognized previously. We recapitulate that this is valid only in the small-angle approximation ($\varphi = 0$); otherwise, two parameters, L and S, are necessary. L_r can be expressed as $1/L_r = 1/L+1/S$, that is, L_r is smaller than either L and S. Therefore, it is sufficient to consider a simple temple-model system with parallel beam.

Thus, equations (3) and (7) (or (8)) are the basic equations of Makyoh imaging: the former gives the position of the image of a given sample point, while the latter gives the image point's illuminance. These equations allow us to calculate the Makyoh image of any surface at a given L.

In some cases, a square grid is projected onto the sample [13, 14] to visualize the large-scale sample deformation. The cells of the grid represent the pencil's cross section upon reflection from the surface. The screen illuminance at a screen point is therefore inversely proportional to the area of the cell image in the screen (see equation (4)). Note also that an additional piece of information is contained in the grid image, since in the illuminance value the shape of the pencil's cross section is lost. Additionally, the grid assists in the direct correspondence between a point of the sample surface and its image.

The one-dimensional case is interesting not only for its analytical transparency, but for the fact that many surface defects possess one-dimensional (line-like or circular) character. The one-dimensional versions of equations (2) and (3) are trivial; they can also be obtained on the basis of simple geometry [15]. The $I(f)$ illuminance at a screen point f will be, as can be obtained from equation (8) or by the differentiation of $f(x)$,

$$I(f) = \rho(x)\left|\frac{\mathrm{d}x}{\mathrm{d}f}\right| = \rho(x)\left|1 - 2L\frac{\mathrm{d}^2h(x)}{\mathrm{d}x^2}\right|^{-1} \tag{9}$$

where x is the sample coordinate.

2.3. Fundamental properties of Makyoh imaging

The imaging is essentially nonlinear, that is, if two surfaces $h_1(\boldsymbol{r})$ and $h_2(\boldsymbol{r})$ produce the corresponding illuminances $I_1(\boldsymbol{f})$ and $I_2(\boldsymbol{f})$, then $h_1(\boldsymbol{r}) + h_2(\boldsymbol{r})$ will not result in $I_1(\boldsymbol{f}) + I_2(\boldsymbol{f})$.

Important scaling relations follow from equations (2) and (7).

(1) Parameters h and L can be scaled as $hL =$ constant; this explains the extreme sensitivity of the method as any small height difference can be detected by increasing $|L|$.
(2) Parameters $\boldsymbol{r}$, h and L can be scaled with the same factor; the image linear size is scaled by this factor, and the screen illuminance by its squared reciprocal.

Equations (3) and (7) tell us that at small $|L|$ a given sample point will be close to its screen image (regarding the sample and the image as being in the same plane) and the image contrast is dominated by the surface reflectivity. Increasing $|L|$ increases the separation of the point and its image, and increases the contrast as well suppressing the reflectivity contrast. As the application of Makyoh is the study of the surface topography, the reflectivity contrast appears as a disturbing secondary effect. At large $|L|$, the L^2 term dominates in the denominator of equation (7), what means that the image of point-symmetry objects will be similar at L's of opposite sign; or, in other words, the sign of surface features cannot be determined. Thus, the optimum setting is in that L range which produces high enough contrast for reliable observation while preserving the integrity of the surface topography.

According to equation (8), the illuminance is infinite if either $L = (2C_{min})^{-1}$ or $L = (2C_{max})^{-1}$, that is, when a screen point is in the focus of an infinitesimal surface area element. For a given reflecting surface, the condition $1/I(\boldsymbol{f}) = 0$ gives the equation of the caustic surface [9], the loci of points of infinite flux. The intersection of the screen with the caustic surface gives the curves of caustics. In one dimension, the condition for caustics is simple (from equation (9)):

$$\frac{1}{2L} = \frac{\mathrm{d}^2h(x)}{\mathrm{d}x^2}. \tag{10}$$

The caustic curve can be a point or an open or closed curve for a given surface depending at what position the screen plane intersects or touches the caustic surface. We show in the appendix that for 'well-behaving' surfaces, if there is a point in the screen image that receives rays from one point of the sample and there is another point that receives rays from at least two different points, there must be a caustic point in the line contacting these two points. This implies that in the non-caustic region of L one screen point receives

reflected rays from only one sample point, that is the image of any two non-overlapping surface areas do not overlap, and a curve which has no intersection with itself is imaged to a curve with no self-intersection. This means, in general, that in the non-caustic region, the surface topology is preserved in the image. In addition, caustics must be avoided because the high illuminance contrast makes the sensing and processing of the image difficult, and interference effects may appear, depending on the coherency of the light source, adding an unwanted complexity to the image. When a grid is applied, caustics can be located as the 'warping' of the image of the grid (see section 4.2 for an example).

2.4. Validity and limits of the geometrical optical approach

In general, diffraction effects are encountered in optics when (1) rays are passed through an aperture and (2) when many rays meet in one point [16, p 370]. In practical Makyoh topography, the first case occurs at the edges of the investigated sample, at non-reflecting surface defects and at surface features that possess abrupt slope changes (e.g. scratches). Assuming Fresnel diffraction at a straight edge, the intensity peak of the first fringe is situated at a distance of $w = 0.875 \times \sqrt{\lambda |L|}$ from the geometrical shadow edge (λ is the wavelength) [16, p 433]; with typical imaging parameters such as $\lambda = 820$ nm and $L = 500$ mm, $w = 0.56$ mm. The extension of the very visible fringes is roughly $5w$. These diffraction features are localized and can be well distinguished from the rest of the image.

The other case happens at caustic points of the image: fringes appear around the caustic points, whose extension depends on the size of the focusing surface feature. We have, however, seen in section 2.3 that the caustic imaging regime is not preferred.

In summary under the usual conditions of Makyoh imaging, the geometrical optical approximation is sufficient; the image contrast changes smoothly.

2.5. Effect of the finite light-source size and the surface roughness

The finite source size can be taken into account as follows. A small Δd shift of the source's position parallel to the sample plane causes a corresponding shift $\Delta d\, L/S$ of the reflected ray in the screen. Thus, the whole image will be convoluted with the weight function $d\, L/S$ where d is the spatial emittance distribution of the light source. It follows from geometrical optics that if the illuminating system consists of a point source placed in the focal plane of a collimator lens whose focal length is F, the convoluting weight function will be $d\, L/F$. The point-source approximation is therefore justified if the characteristic size of the surface features is larger than the width of the convoluting weight function. In camera-based systems, $L \approx -F$ [11], that is, the lateral resolution of the imaging roughly equals the extension of the source. Note further that as long as the conditions for the geometrical optical approximation (see previous section) hold, the geometrical optical treatment remains valid for the extended source as well, since the source is subtended by a small angle at a given surface point; thus, the source's finite extension does not corrupt the smoothness of the reflected beam's intensity profile.

On the basis of equation (2), the surface roughness influences the image through the surface's slope distribution [17]; the image is convoluted with $2L$ times the slope distribution function.

As the lateral resolution deteriorates with increasing $|L|$ in both cases discussed above, these factors may limit the ultimate sensitivity of the method in practice.

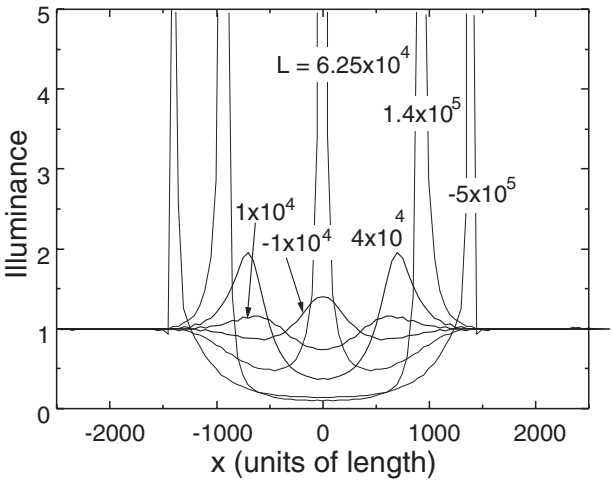

Figure 2. Simulated images of a hillock at different L settings.

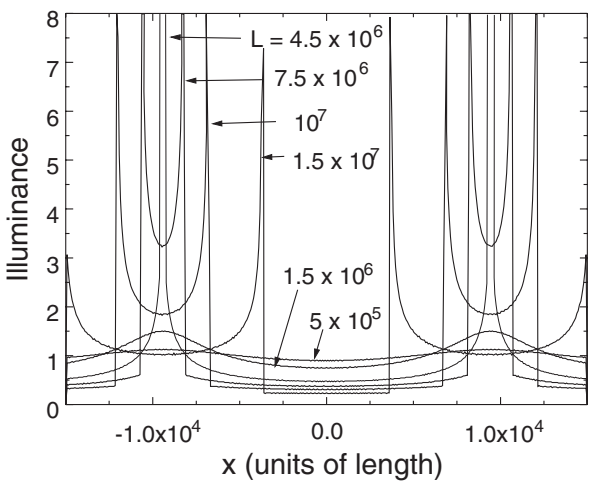

Figure 3. Simulated images of a sinusoidal surface at different L settings.

3. Simulation results

3.1. Simulation method

The computer code used for the simulations scans the $h(x)$ values in equidistant steps of x, then the $f(x)$ values and corresponding $I(f)$ illuminance values, as calculated from the one-dimensional version of equation (3) and equation (9), are stored in an array from which the final $I(f)$ profile is calculated after scanning the whole range of interest of x (the simple 'ray counting' approach [15] which does not take into account the intensity of the individual rays gives

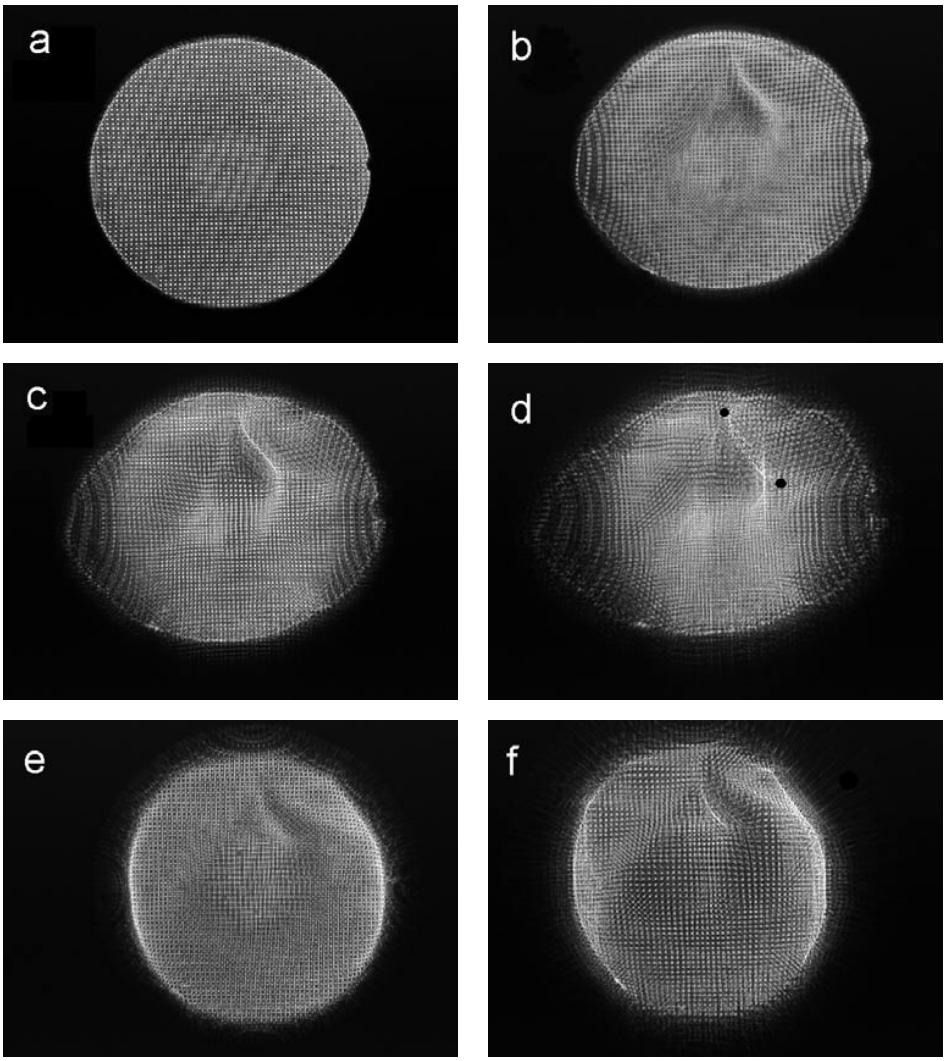

Figure 4. Makyoh images of a Si wafer. The wafer diameter is 24 mm. Experimental conditions: (a) $L = 0$, (b) $L = -63$ mm, (c) $L = -190$ mm, (d) $L = -375$ mm, (e) $L = 198$ mm, (f) $L = 400$ mm.

the same result if the density of rays is large enough). We assume that the surface reflectivity is unity over the whole X range. All lengths are expressed in arbitrary units. Our approach has the advantage over the MC simulation [7] of the production of a real intensity profile that can be manipulated further or compared to experimental profiles etc; the MC simulation gives only an image composed of individual dots corresponding to the rays impinging on the screen.

3.2. Hillock and depression

We model a hillock with a Gaussian profile:

$$h(x) = A \exp[-(x/k)^2].$$

This is a first approximation for any small isolated defect on a flat surface. Based on the scaling relations (see section 2.3), we change only L and fix $A = 1$ and $k = 500$. A depression is modelled by altering the sign of L. The image is, typically, a dark (or light) band surrounded by a pair of light (dark) bands (figure 2). This can be understood also by approximating the hillock as a convex mirror on a flat surface [11]; the image results from the focusing or defocusing of the beam reflected from the hillock, depending on the relation between the feature's focus and L. The sharpest focusing occurs at $L = -6.25 \times 10^4$. At large $|L|$, the images are similar (a dark spot) for negative and positive L: in this case, the rays reflected from the hillock are totally scattered out of the image, being distributed over a large area. Caustics appear at the edges at $L = 1.4 \times 10^5$ due to the focusing effect of the concave tails of the Gaussian profile.

3.3. Sinusoidal surface

A sinusoidal profile may model any periodic or quasi-periodic surface. The surface is described as $A \cos kx$. Based on the scaling relations, we fix $A = 1$ and $k = 1/3000$ and vary L. Because of symmetry, only positive L values are considered. Figure 3 shows the results. At small L values, the image closely reflects the surface profile, but the contrast is small. Increasing L yields increasing contrast, and the intensity profile becomes sharper producing peaks due to the alternating focusing/defocusing effect of the periodic profile. The caustic limit, based on equation (10), is reached

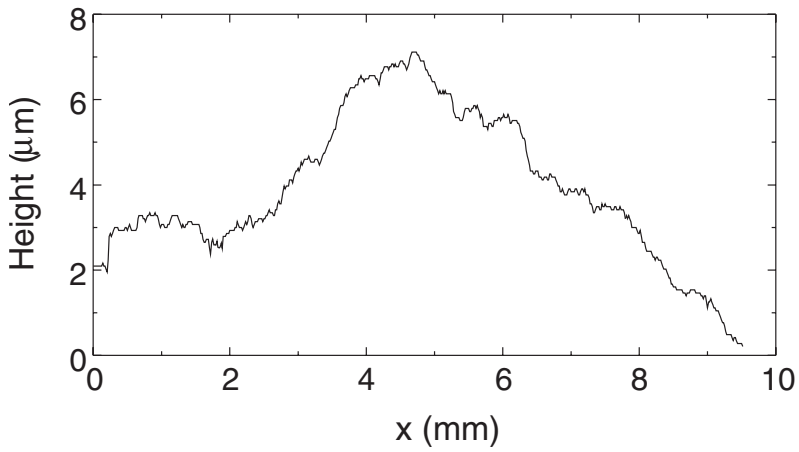

(a)

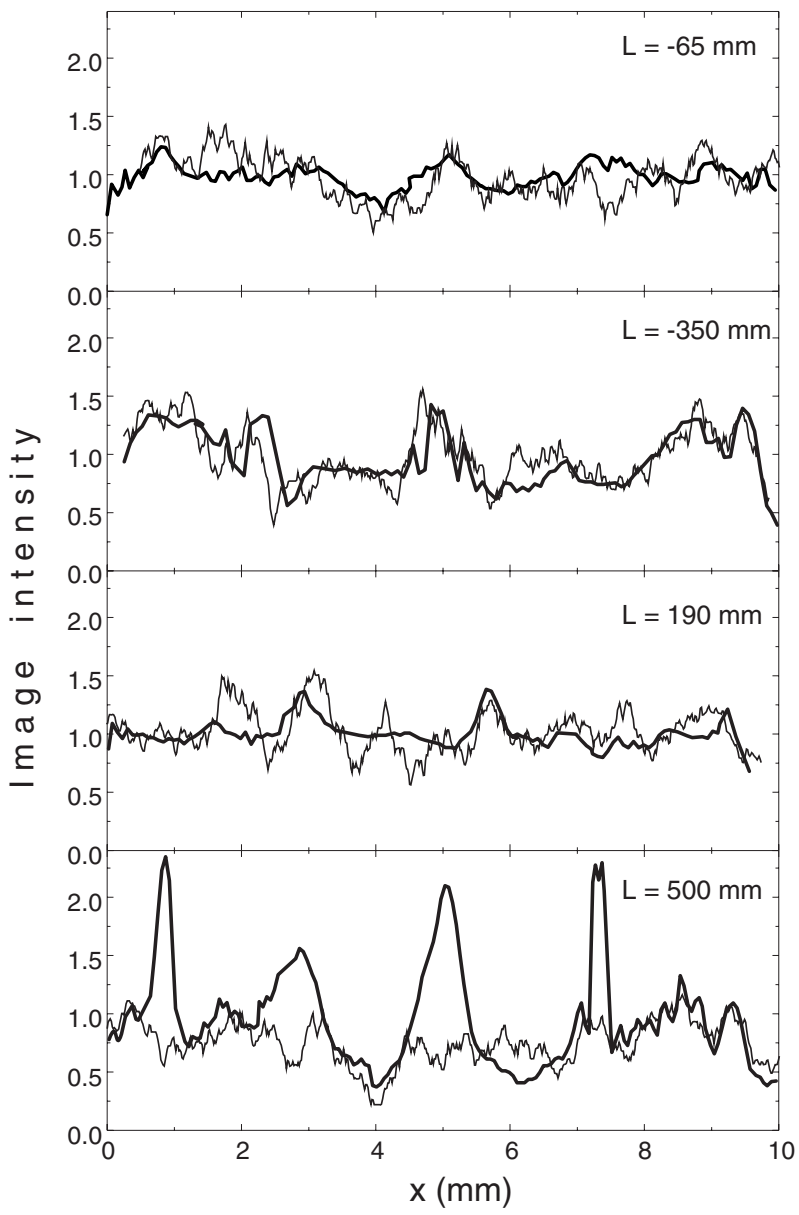

(b)

Figure 5. (a) Surface stylus scan of a section of a corrugated plastic plate; (b) measured (thick curves) and simulated (thin curves) Makyoh images of the plate at different L settings.

at $L = 1/(2Ak^2) = 4.5 \times 10^6$; at higher L's, the peaks split and separation of the split parts increases.

4. Experimental results and discussion

4.1. Makyoh instrument

In our Makyoh equipment [10, 11], the light source is a pigtailed LED operating at 820 nm wavelength providing a 50 μm diameter point source. The emitted light power can be regulated from zero to about 60 μW. The additional optical system consists of a large-diameter collimating/magnifying lens (focal length, 500 mm) placed a few centimetres above the sample. The light source is placed in the focal plane of the collimator lens, that is, the light beam is closely collimated. The camera is a 800×600 pixel resolution black and white CCD camera. The camera video output is fed to a 8 bit frame grabber card inserted into a personal computer with appropriate image-processing software. In the present experiments, we used a 35 mm focal length camera lens. The value of L can be varied from -750 mm to 500 mm using different camera lens distance settings and extension tubes.

4.2. Makyoh images and discussion

We selected two samples for the present study: a Si wafer patterned with metal dots to illustrate the main principles and to show a realistic situation, and a one-dimensional model surface to quantitatively check the model.

Figure 4 shows the Makyoh images of the Si wafer at different L settings. The patterning imitates the projected grid. The images taken with different L's show that the more dense the grid image, the higher the image brightness, according to the note at the end of section 2.2. Higher $|L|$ setting causes larger image contrast and stronger distortion of the grid image, and, in general, a more structured image. The evolution of a caustic curve can be followed in the upper right part of the images. In figure 4(b), a bright curved line can be seen, but the caustic limit has not yet been reached. The caustic limit is just passed in figure 4(c), as shown by the bright, narrow line and the onset of the warping of the grid image; then, the grid image becomes warped (figure 4(d)), indicating that the domain enclosed by the caustic curve receives rays from different parts of the sample (the caustic curve is marked by two black dots in figure 4(d)). Note the role of the sign of L: the images of the same area shows opposite intensity at opposite-sign L settings.

As the model surface, we selected a flat plastic plate that exhibits a one-dimensionally corrugated surface probably due to the imperfect fabrication process. Gold was evaporated on the plate to obtain a reflecting surface. The surface profile was measured by a surface stylus profilometer equipped with a translation stage and computer-based data acquisition. Figure 5 shows the measured surface scan and the Makyoh image profiles together with the corresponding profiles simulated using the measured scans. To reduce noise, 64 images were integrated to get one profile. Note that the magnification and the image intensity changes with L; these effects have been corrected and the relative intensity as defined in section 2.1 is shown in figure 5. The agreement between the simulations and the measurements is satisfying, considering the following possible sources of error: (1) the reflectivity of the gold layer has an approximately 5% fluctuation with a characteristic period of a few tens of micrometres; (2) the surface stylus scan acquires some fluctuations because of the vibration of the stepping motor of the translation stage. These factors cause unpredictable deviations in the simulated profiles, especially at large $|L|$. This might be responsible for the lack of reproduction of the measured peaks in the $L = 500$ mm image.

5. Conclusions

In conclusion, we have presented a comprehensive geometrical optical model for the image formation in Makyoh topography. Fundamental properties of the image formation were established. Simulations for some practically important cases were performed. The basic principles were demonstrated using observed Makyoh images of a semiconductor wafer, and the model was checked quantitatively.

Acknowledgments

The original Makyoh instrument was built by J Szabó and J Makai, the computer-based video system is due to I Eördögh; these contributions are gratefully acknowledged. The author is also grateful to B Szentpáli for encouragement, to B Pödör for the critical reading of the manuscript, to J Mizsei for the surface stylus profiles and to J Bernges (RWTH Aachen) for his kind interest in this work and for drawing the author's attention to references [8] and [9]. This work was supported, in part, by the (Hungarian) National Scientific Research Fund (OTKA) through grant No F 25224, by the European Union under contract No 977131 (MEMSWAVE), and by the János Bolyai Postdoctoral Research Scholarship of the Hungarian Academy of Sciences.

Appendix

We prove that if there is a point A in the image plane that is illuminated by a ray from one point of the sample only and there is another point (point B) that is illuminated by rays coming from at least two distinct points of the sample, then there is a caustic point in the line AB, provided that the first and second derivatives of $h(\boldsymbol{r})$ are continuous (see figure A1). It follows then that a continuous curve of the sample surface is imaged to a continuous curve in the image. Now, let B_1 and B_2 those points of the sample surface from which B receives the rays. Let H be that point on the line AB for which it holds that all points of HB receive two rays and all points of AH receive only one ray. (If these kinds of sections alternate, the closest border point to B is taken as H.)

Since a continuous curve is imaged to a continuous curve, the line HB is the image of two continuous curves, H_1B_1 and H_2B_2. H_1 and H_2 coincide, since a point in the line AH that is infinitesimally close to H must be the image of a sample point that is infinitesimally close to both H_1 and H_2. Let u and v be the curvilinear coordinates along

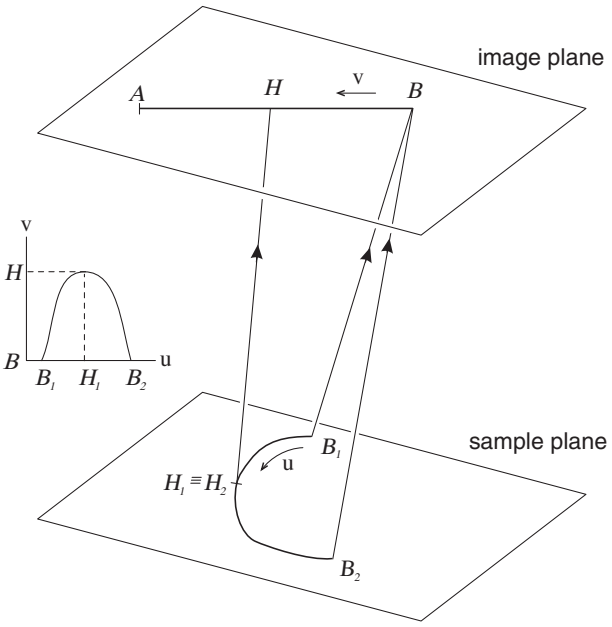

Figure A1. Illustration of the proof.

$B_1H_1B_2$ and BH, respectively. Since $v(B_1) = v(B_2)$ and $v(u)$ is continuous, $v(u)$ must have a maximum at $u = H_1$. On the other hand, as dv/du is continuous as well, dv/du must be zero at the maximum ($u = H_1$), therefore du/dv must be infinite at $u = H_1$; that is, H is a caustic point (see the inset in figure A1).

It follows also from this proof that a caustic curve that is associated with a multiple-irradiated point (like B) is closed or ends at the image of the sample border. Caustic domains my overlap as well. Furthermore, it can be shown that if we relax the continuity of the second derivatives of $h(\boldsymbol{r})$, the points of type H will not have infinite illuminance; if the first derivatives are allowed to be non-continuous, the continuous lines may not be imaged to continuous lines (the image contains dark areas).

References

[1] Bragg W 1933 *The Universe of Light* (London: Bell) p 35
[2] Owaga T (ed) 1990 *Proc. 3rd Int. Symp. on Defect Recognition and Image Processing in III–V Compounds (DRIP III)*, *J. Cryst. Growth* **103** 420–68
[3] Blaustein P and Hahn S 1989 *Solid State Technol.* **32** 27
[4] Németh-Sallay M, Minchev G M, Pödör B, Pramatarova L D, Szabó J and Szentpáli B 1993 *J. Cryst. Growth* **126** 70
[5] Laczik Z, Booker G R and Mowbray A 1995 *J. Cryst. Growth* **153** 1
[6] Okabayashi O, Shirotori H, Sakurazawa H, Kanda E, Yokoyama T and Kawashima M 1990 *J. Cryst. Growth* **103** 456
[7] Korytár D and Hrivnák M 1993 *Japan. J. Appl. Phys.* **32** 693
[8] Burkhard D G and Shealy D L 1973 *J. Opt. Soc. Am.* **3** 299
[9] Shealy D L and Burkhard D G 1973 *Opt. Acta* **20** 287
[10] Riesz F 2000 *J. Cryst. Growth* **210** 370
[11] Szabó J, Riesz F and Szentpáli B 1996 *Japan. J. Appl. Phys.* **35** L258
[12] Oprea J 1997 *Differential Geometry and its Applications* (New York: Prentice-Hall)
[13] Szabó J, Riesz F and Szentpáli B 1995 *Mater. Res. Soc. Symp. Proc.* **379** 103
[14] Yang K H 1985 *J. Electrochem. Soc.* **132** 1214
[15] Riesz F 1999 *Phys. Status Solidi* a **171** 403
[16] Born M and Wolf E 1964 *Principles of Optics* 2nd edn (Oxford: Pergamon)
[17] Bennett J M and Mattsson L 1989 *Introduction to Surface Roughness and Scattering* (Washington, DC: Optical Society of America) p 44